Proceedings World Geothermal Congress 2020+1
Reykjavik, Iceland, April - October 2021

Geothermal Exploration With Ambient Noise Tomography, Gravity Data and a 3-D MT Resistivity Model in a Joint Inversion Approach

Jean-Michel Ars[a], Pascal Tarits[a,b], Sophie Hautot[b], Mathieu Bellanger[c], Olivier Coutant[d] and Marci Maïa[a]

[a] IUEM, UMR 6538 Laboratoire Geoscience Ocean, Plouzané F29280, France

[b] IMAGIR Sarl, Saint-Renan F29290, France

[c] TLS-Geothermics, Toulouse F31200, France

[d] Université Joseph Fourier, UMR 5275 ISTerre, Grenoble F38041, France

jean-michel.ars@univ-brest.fr

Keywords: Joint Inversion, Geothermal, Magnetotellurics, Gravity, Ambient Noise Tomography, Exploration, Unconventional Geothermal Reservoir, Fault

ABSTRACT

Geophysical exploration of unconventional geothermal resources is challenging due to the lack of any well-known specific geophysical signature such as the clay cap observed in volcanic geothermal systems. Moreover, unconventional geothermal reservoirs usually set in a complex geological environment. In this context, geophysical models should provide some image at a scale large enough to understand the complex geology but with the adequate resolution to resolve features like faults. One solution to overcome this difficulty is to use jointly several geophysical methods providing complementary insight into the geology.

We developed a joint inversion technique of gravity and ambient noise tomography constrained by a resistivity model from a prior 3-D MT inversion. This approach was first applied to data collected for the geothermal exploration of a prospect in a crustal fault zone located in Massif Central, France. In 2017, a dense temporary seismic network with 299 vertical component geophones was installed in the area. We present the joint inversion of this new seismic data set with MT and gravity data.

The geophysical data set consists of 48 MT soundings, 627 gravity measurements, and 579 surface wave dispersion curves. We first inverted the 48 full MT tensors to obtain a 3-D resistivity model. We then jointly inverted the gravity data and the surface wave dispersion curves with our 3-D approach. The 3-D resistivity model constrains the joint gravity and seismic solution. Couplings between resistivity, density and shear wave velocity models are based on linear correlations. Such a global coupling inversion strategy allows models to be sufficiently unconstrained locally to fit the data while being able to converge toward a solution with correlated parameters within some of the geological domains.

1. INTRODUCTION

Unconventional geothermal reservoirs can set in various geological contexts (fractured basement, sedimentary basin) from a large range of heating source (upwelling asthenosphere, high radioactivity of the crust) (Moeck, 2014). These reservoirs modify sub-surface physical properties in different ways. It is the combination of complementary information in particular from several geophysical techniques that allows to identify the specificities of each geothermal resource (Gola et al., 2017). In order to investigate this approach, we developed a joint inversion technique of gravity and ambient noise tomography (ANT) constrained by a resistivity model from a preliminary standalone 3-D MT inversion (Ars et al., 2019). The three geophysical methods provide complementary insight into the geology since MT is sensitive to fluid and mineral phases, ANT is controlled by structural properties, and gravity maps the lithology. We choose to jointly invert the gravity and the seismic data set under the constraint of the MT model. Resistivity, density and Vs velocity parameters are coupled through linear correlation laws. Instead of assuming petrophysical relationships between geophysical parameters, we try to enforce their correlation in order to emphasise geological features locally. This approach was first applied for the geothermal exploration of a prospect in a crustal fault zone located in the Massif Central, France (Ars et al., 2019). In that study, the seismic ambient noise tomography data were limited to a 2-D profile. In 2017, a dense temporary seismic network with 299 vertical component geophones was installed in the area and the resulting surface wave dispersion curves included in the joint inversion with a refined MT and gravity network of data.

The geological context comprises a granitic body and a metamorphic unit facing each other on both sides of a valley. The setting of the granitic body on the west of the valley would be associated to a major fault zone (MFZ) (Bellanger et al., 2017), permeable enough for deep fluid circulation (Roche et al., 2017). Ars et al. (2019) propose a location in-depth for this fault zone and a heat anomaly marker in depth along with a West-East 2D profile. In this study, we aim to describe the 3-D geometry of the faulting zone. In the following, we present the data acquisition and processing. We detail the data inversion in two steps, first the MT inversion then the gravity and seismic joint inversion constrained by the resistivity model. Models are finally discussed in terms of unconventional geothermal exploration.

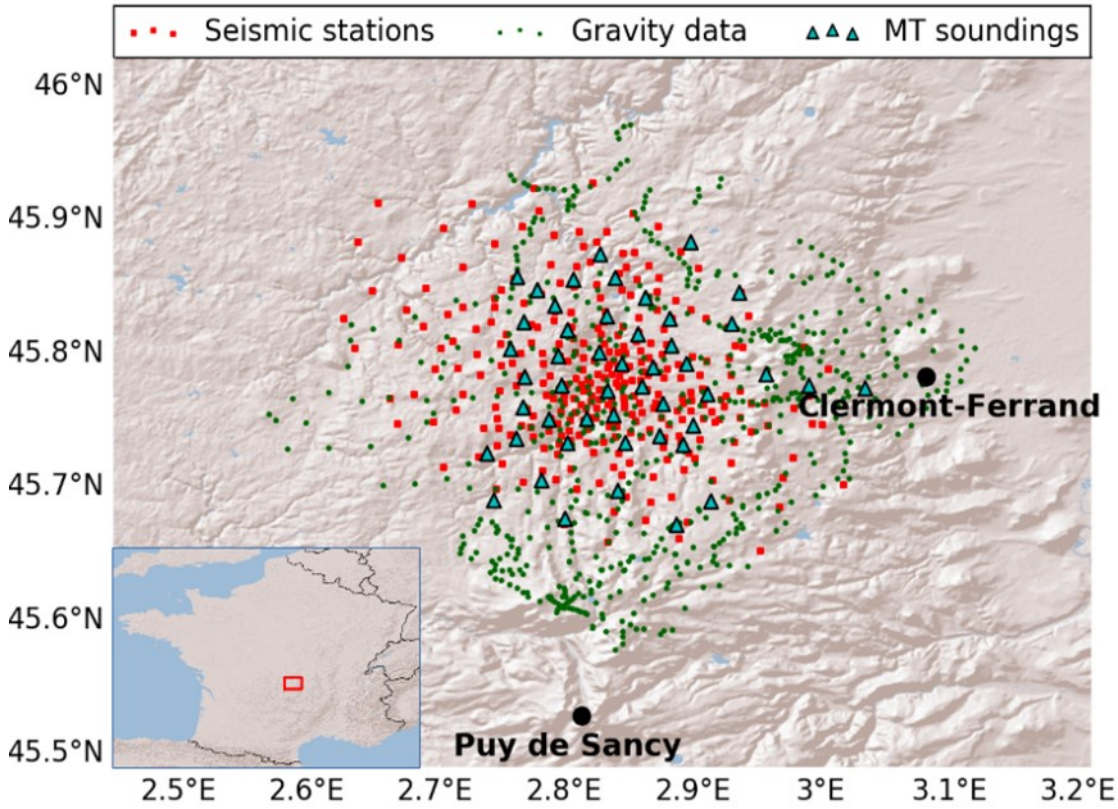

Figure 1: Geophysical survey map of the study. Location of the survey area (French Massif-central) is shown on the France map on the lower-left corner of the figure.

2. GEOPHYSICAL SURVEY

2.1 Seismic Ambient Noise Data

A dense temporary seismic network of 299 vertical component geophones was deployed in 2017 from November 6th to December 7th (32 days). The geophones were set on a non-regular 30km x 30km grid (Figure 1). The seismic sensors used for the survey are Fairfield Nodal Zland nodes. The correlation functions between all couples of nodes were computed from the daily seismic ambient noise recording (Shapiro and Campillo, 2004). We obtained 44,551 Rayleigh wave group velocity dispersion curves from correlation using a frequency-time analysis (Levshin et al., 1989). We rejected all the dispersion curves for station pairs separated by less than one wavelength to avoid larger uncertainty measurements. We also rejected at each period the group velocity measurements greater than the most probable velocity, more or less 0.5 km/s. We thus obtained robust dispersion curves with a period ranging from 0.9 to 4.7 seconds. Group velocities were inverted into Rayleigh wave group velocity maps in the period range 0.9-4.7s using Mordret et al. (2014) approach. The maps were finally sampled on a regular grid every 700m in both horizontal directions. The final data set consisted of 921 local dispersion curves covering the area limited by the seismic array.

We compared the group velocity maps obtained from the dense seismic network with the dispersion maps from the previous study (Ars et al., 2019) where the ANT was performed using 11 broadband seismic stations in the same region. Ambient noise recordings from this sparse seismic array were identically processed into Rayleigh group velocity maps and local dispersion curves for a period ranging from 2.5 to 10 seconds. Both tomography studies have two different ranges of the period because of the different seismic sensors used for each survey. Thus, we compared the group velocity maps only for the common period range 2.5-4.5s. Due to the cross-shaped network of the first seismic survey (Ars et al. 2019) and the bidirectional sources of noise (North Atlantic and Mediterranean sea), dispersion maps of the former study are only resolved along with a roughly East-West profile (see Figure 2). The seismic profiles show group velocity gradient increasing from East to West in agreement with the velocity maps obtained with the dense network in terms of structure and velocity range.

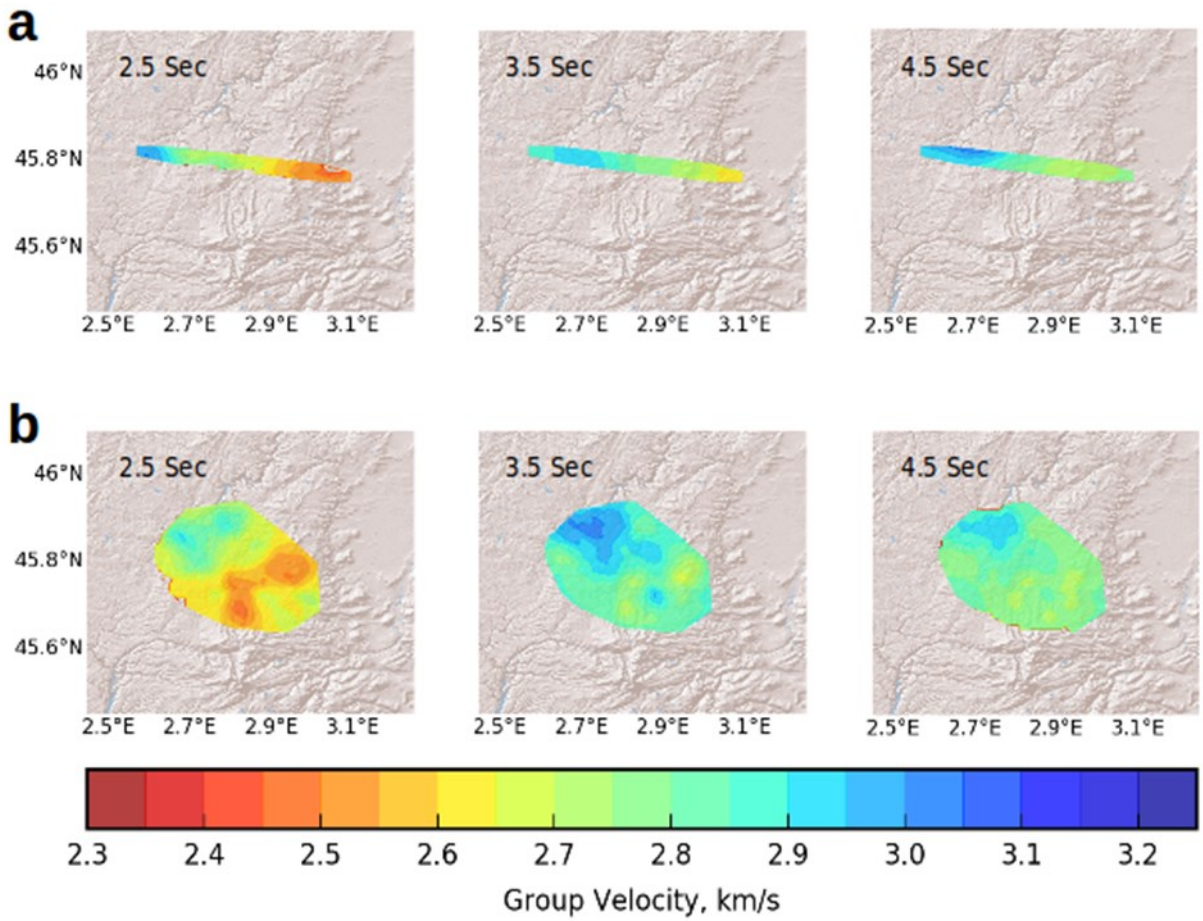

Figure 2: Group velocity dispersion maps from a) the 11 broad-band seismic stations network and b) the dense temporary network. Group velocity maps are displayed for a period ranging from 2.5 s to 4.5s.

2.2 Magnetotelluric Data

We first carried out 45 magnetotelluric (MT) soundings in September 2015, then complementary 4 and 18 MT soundings were added to the data set in September 2016 and 2017 for a total of 67 MT soundings. In this study, we analysed 48 MT soundings overlaying the seismic network, homogeneously distributed over an area of 23 km x 23 km (Figure 1). MT data acquisition was performed using Metronix equipment. Horizontal electric fields were recorded using pairs of unpolarised Pb-$PbCl_2$ electrodes 100 meters apart in average, and magnetic fields were recording using MF-07 and MF-06 coils. A typical impedance tensor of the MT survey is presented in Figure 3. This site is representative of the abnormal behaviour of many impedance tensors. Indeed, most of the MT tensors display large apparent resistivity values for the diagonal components over one second, and some tensors are characterised by off-quadrant off-diagonal phases at long periods.

2.3 Gravity Data

A total of 90 gravity measurements were performed with a SCINTREX CG-5 gravimeter (Ars et al. 2019) and completed with 537 gravity points from the International Gravity Bureau (IGB) data set for a total of 627 absolute gravity data. We computed the complete Bouguer anomaly using the DEM from ASTER GDEM 30m (NASA, 2009) and a reference density of 2670 kg/m^3. We also computed a regional Bouguer anomaly with a large data set of values from IGB. The regional anomaly represents the large-scale effect of the Massif-Central uplift related to its recent volcanic activity (Granet et al. 1995). Extracting this regional trend at the scale of the study was equivalent to remove the mean value. The residual Bouguer anomaly is presented in Figure 4. We observe a W-E increasing trend with a low Bouguer anomaly associated with the granitic body and a high Bouguer anomaly associated with the metamorphic unit and the volcanism.

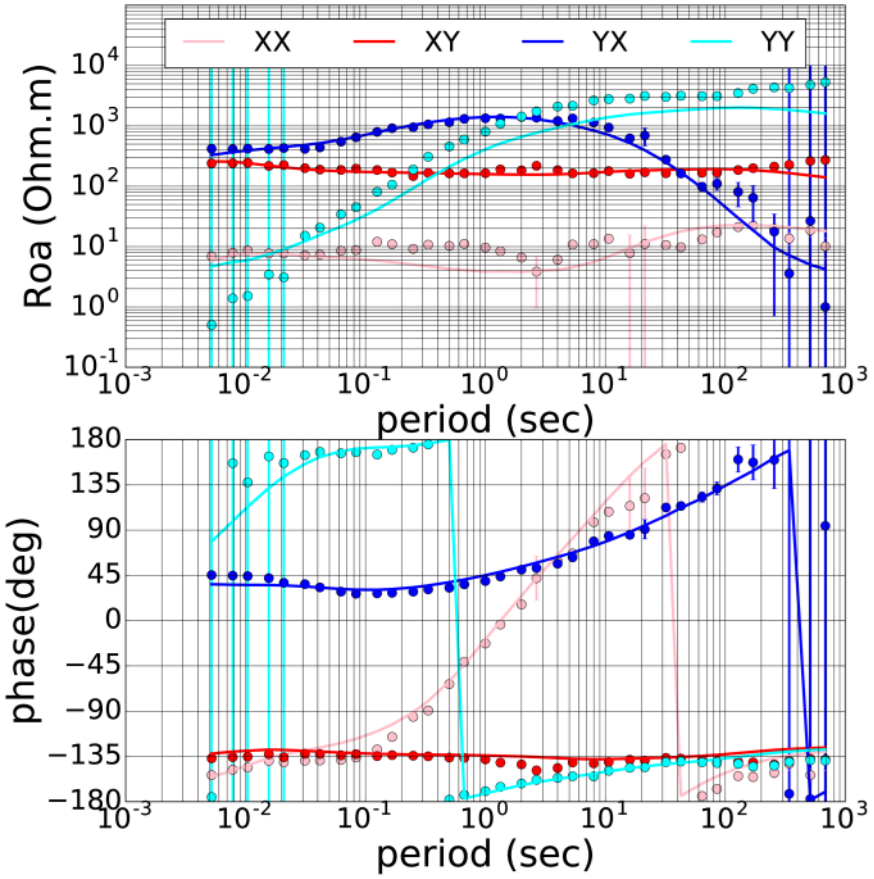

Figure 3: Example of impedance tensor. Apparent resistivity of the four components of the tensor is shown on the upper panel while the lower panel displays the phase. Data are represented with dots. We superimposed the response of the best fitting model with continuous lines.

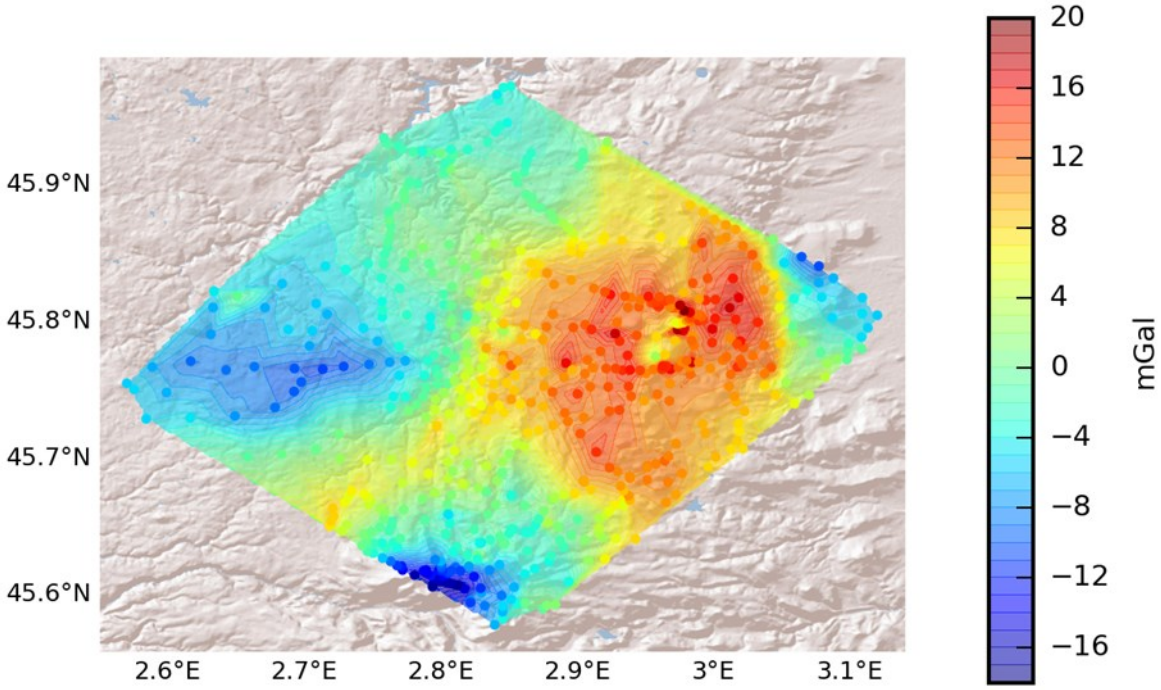

Figure 4: Map of the residual Bouguer anomaly.

3. GEOPHYSICAL INVERSION

3.1 Magnetotelluric Inversion

We performed the 3-D MT inversion using the inversion software MINIM3-D (Hautot et al., 2000, 2007). MINIM3-D is an iterative process that minimises an objective function, composed of a data misfit term and a regularisation term, using a non-linear steepest gradient method (Beiner, 1970; Press et al., 2007). We inverted the 48 full impedance tensors for all periods available. MT impedance tensors were inverted into a resistivity model made of 28 x 26 x 15 cells (North 130° x East 40° x Depth) covering an area of 39.1 km x 41.4 km down to 51.2 km depth. As aforementioned, some impedance tensors have off-quadrant off-diagonal phase as well as large diagonal apparent resistivity values. Such impedance tensors may be interpreted in terms of anisotropic electrical medium or of highly contrasted resistivity structures related to a strong rotation (> 90°) of the structure's strikes with depth (Pina-Varas & Dentith, 2018). We choose to model the data with an isotropic 3-D model. In order to optimise the 3-D inversion of the full MT data set, we performed a 3-D local inversion analysis on each impedance tensors that allow to determine the optimum grid orientation. A rotation of 40°N of the grid proved to be optimum to model the complex phases behaviour accurately. The model parameters are the resistivity in each grid cell. In order to reduce the number of parameters, cells are grouped with depth in accordance with the data distribution and the loss of resolution. The parametrisation led to 3,268 unknowns for 11,866 data (real and imaginary part of the four terms of the impedances tensors at every period available). The minimum error floor used on the data is set to 1.5% and 5% on the off-diagonal components and the diagonal components of the tensors respectively, while the maximum is the standard deviation. The root mean square (RMS) of the final model is equal to 3.6. Responses of the final resistivity model fit the data and reproduce correctly the complex behaviour of the impedance tensor, particularly the off-quadrant off-diagonal phases. A typical example of the fit between the model responses and the data is given in Figure 3.

3.2 Joint Inversion

We run the joint inversion of the gravity and seismic ambient noise data using the joint inversion algorithm developed by Ars et al., 2019. The joint inversion is an iterative process that minimises an objective function using a non-linear steepest gradient method (Beiner, 1970; Press et al.,2007). The objective function is composed of two misfit functions, one for each geophysical data (gravity and seismic), that measure the discrepancy between the model responses and the data. Model responses are computed using the forward gravity solution from Blakely (1996), and the dispersion curve computation from Wathelet, (2005). It also contains one regularisation terms for each geophysical method and three coupling terms. Coupling terms allow constraining common features between geophysical models. They are based on the correlation of the model parameters: resistivity, density and Vs velocity (Ars et al. 2019). Finally, the resistivity remains constants through the inversion.

Gravity data are inverted for a 3-D density model while the local dispersion curves are inverted for a 1-D shear wave velocity (Vs) model. All 1-D velocity profiles are stitched into a pseudo-3-D velocity model to compute the coupling terms with density and resistivity. To optimise the coupling between models, the density and the Vs velocity model have the same orientation (N40°) and the same extension as the resistivity model. The density model is made of 28 x 26 x 15 cells (North 130° x East 40° x Depth). The lateral griding of the density model is identical to the resistivity grid covering an area of 39.1 x 41.4 km down to 14.7 km. The maximum depth of the density griding is chosen to be equal of the half of the gravity data extension. The velocity model is made of 38 x 36 x 12 cells. The lateral griding is homogeneous (1150 x 1150 meters) and coincide in the centre with the density griding. The velocity model covers an area of 39.1 x 41.4 km down to 6 km. The maximum depth of the seismic griding was determined by a stochastic inversion of the mean dispersion curve. Resistivity-velocity and density-velocity coupling terms are computed in accordance with the seismic griding, while the resistivity-density coupling term is computed in accordance with the gravity griding. Considering that the seismic model is the shallowest, the volume constrained by the three coupling terms is restricted to the volume occupied by the velocity model.

We inverted 627 gravity data and 579 local dispersion curves at all periods available, ranging from 0.9 to 4.7 seconds. The number of dispersion curves used for the inversion is lower than the total number of available dispersion curves because it corresponds to the optimum number of dispersion curves to fit one seismic data in each column of the oriented velocity griding. Thus, we run the joint inversion for 10,920 density parameters and 7,527 velocity parameters for a total of 22,050 data (all gravity measurements and group velocities at every period available). The standard deviation used on the data is set respectively to 1 mGal and 100 m/s on the gravity and the seismic data. The initial density contrast model is homogeneous and equal to 0.0 kg/m^3 while the initial Vs velocity model is a vertical gradient increasing from 3000.0 m/s on the surface to 3600.0 m/s in-depth. The final gravity RMS is 0.807 mGal, and the final seismic RMS is 48.125 m/s. Seismic and gravity models responses fits are presented in Figure 5. The gravity fit between the model responses and the data is generally good, except near topography highs. The dispersion curves responses fit well the data, with every local RMS less than 100 m/s. The western part of the model presents a very good fit with every local RMS less than 60 m/s. Only the dispersion curves located in the centre of the survey area displays RMS greater than 80 m/s due to long period slight split, which implies uncertainties on the deep velocity around this area. However, these are 1-D fits between local dispersion curves and 1-D model responses. The pseudo-3-D velocity model is composed of 1-D Vs model stitched together, but the 3-D nature of the final Vs model cannot be verified with a real 3-D forward solution. We rely on the coupling terms to bring constraints on the Vs model from the 3-D resolved gravity and MT models.

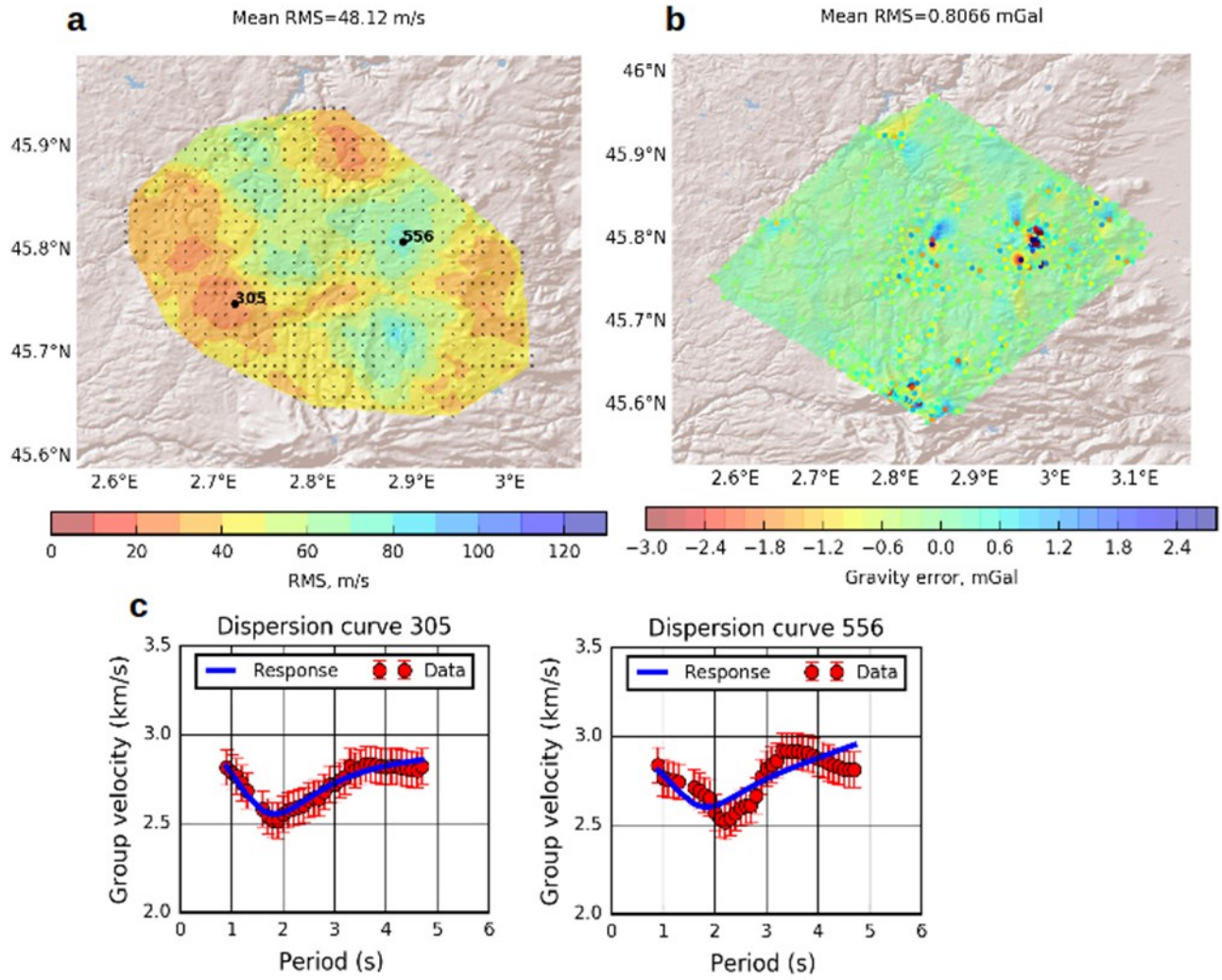

Figure 5: a) Map of the seismic RMS for each dispersion curves, b) map of the gravity RMS point by point, c) two example of local dispersion curve fits, data are represented with red dots and model response with the blue line.

3.3 Results

Figure 6 displays the resistivity model from the 3-D MT inversion, the density and the velocity models from the 3-D joint inversion. We will only comment on the result for the common part of the three models where they are actually all coupled together. It corresponds to the volume occupied by the velocity model down to 6km. Models are shown for three different layers approximately at the same depth for each model: ~ 0.5-1 km, ~ 2.0-2.5 km and ~ 4.5-5.0 km.

The final correlation between density and resistivity, and Vs velocity and resistivity are respectively 0.14 and 0.28, while the final correlation between density and velocity is 0.43. These correlation values are small but global. They are statistically significant (p-value is lower than 10^{-10} for each coupling term), and it indicates that some parts of the model are correlated to each other, not necessarily for the whole model. Indeed, the average model scale correlation between density and velocity locally increases in accordance with the local geological unit. The local correlation corresponds in the models to a low-velocity structure correlated to a low-density structure on the west of the major fault zone (MFZ, Figure 6). The correlated parameters correspond to the location of the granitic body and it extents in depth. However, density-velocity correlation is less obvious elsewhere in the model. The east of the MFZ is characterised by high-density structures that may be related to metamorphic units, but they are not correlated with high-velocity values (Figure 6c). Similarly, even if the velocity-resistivity correlation is low, they may be locally correlated and be a marker of very heterogeneous geological features. For instance, small low-velocity structures scattered along the MFZ seem to be correlated with small conductive bodies in the same area for depth greater than 2 km. Those correlated parameters seem to be related to the location of the MFZ. They may reveal local alteration such as fracturing or presence of water that might locally decrease the resistivity and the velocity. A fractured zone may have the same implication in term of geophysical signatures for the MT and the ambient noise tomography, but it seems not to affect the gravity signature the same way. Where resistivity and the velocity seem to be correlated along the MFZ, density distribution does not evolve similarly. Indeed, MT and seismic models shape the MFZ with low parameters anomaly while the MFZ is associated with a transition zone within the density model. This behaviour explains the very low correlation between resistivity and density there.

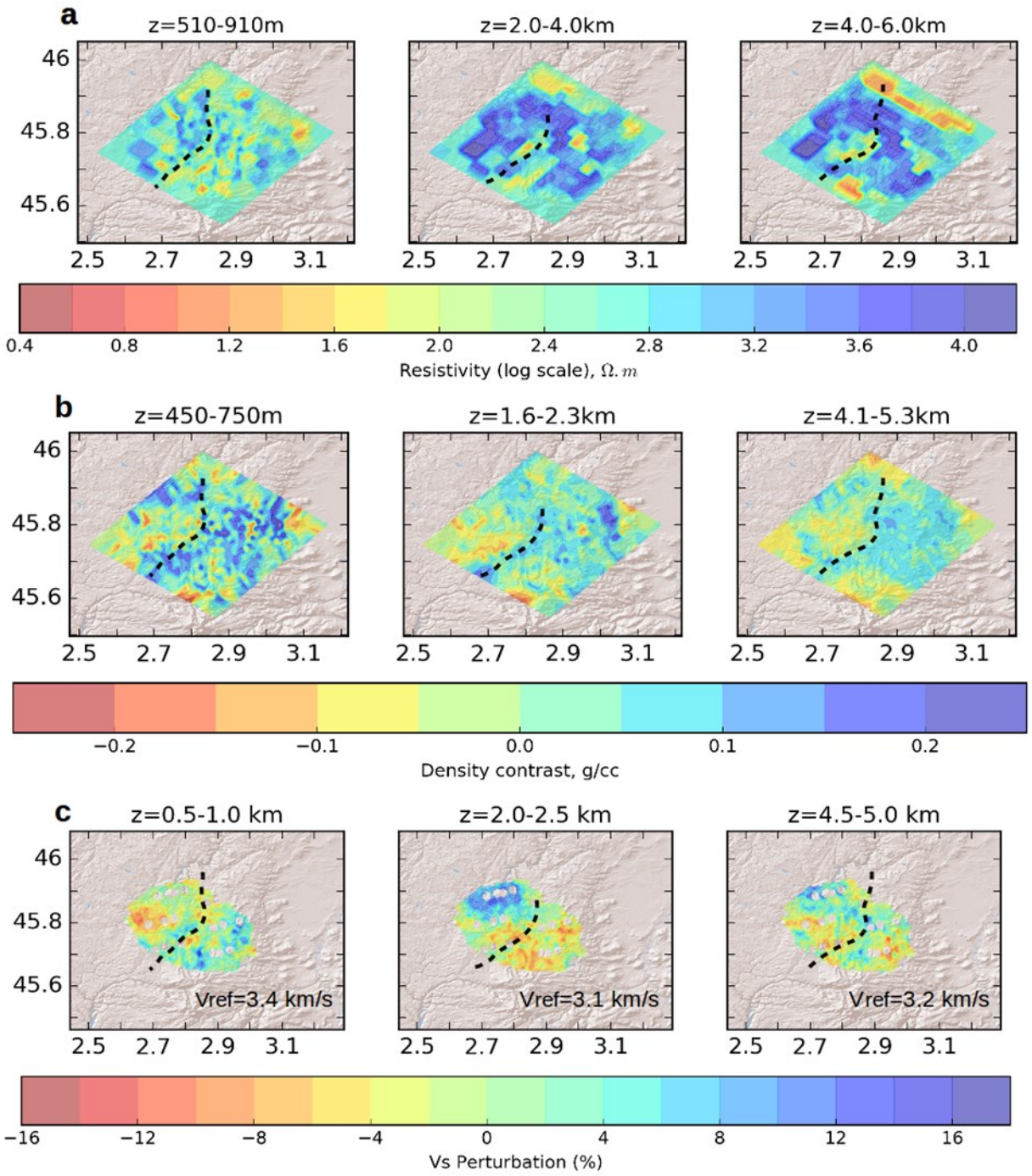

Figure 6: a) Resistivity distribution for three different layers. b) Density contrast distribution for three different layers. c) Vs velocity anomaly relative to a reference velocity for three different layers. The major fault zone is represented on each layer with the black dashed line.

4. CONCLUSION

The growth of unconventional geothermal exploitation strongly relies on the ability to perform a reliable exploration of heterogeneous geological features such as faults. The integration of complementary geophysical methods enhances a conceptual model but is limited due to the partial inconsistency between geophysical techniques. Moreover, geothermal exploration in complex geological contexts requires a large number of data to cover an area wide enough to understand the regional geological trend, with a good resolution to image small target. In order to improve geophysical exploration for an unconventional geothermal system, we presented a joint inversion approach of MT, gravity and ambient noise tomography dense data set from the French Massif-Central. MT data are first inverted into a resistivity model used as a frozen constraint for the joint inversion of the gravity and seismic data. Coupling terms between models are computed with linear correlation law and intensify local linear relation between parameters that are related to geological features. We thus propose that a major fault zone in the survey area is highlighted as a density contrast transition and a low velocity and low resistivity anomalies. This result seems to indicate that linear correlation coupling is the first

step for fault imaging but is not efficient enough. We need to develop non-linear coupling terms to model such heterogeneous structures.

ACKNOWLEDGEMENTS

We would like to acknowledge the International Gravity Bureau for providing us with the necessary gravity data.

REFERENCES

Ars, J. M., Tarits, P., Hautot, S., Bellanger, M., Coutant, O., & Maia, M.: Joint inversion of gravity and surface wave data constrained by magnetotelluric: Application to deep geothermal exploration of crustal fault zone in felsic basement, *Geothermics*, **80**, (2019), 56-68.

Blakely, R. J.: Potential theory in gravity and magnetic applications, Cambridge University Press (1996).

Beiner, J.: FORTRAN routine MINDEF for function minimization. Institut de Physique, Univ. of Neuchatel, Switzerland, **65**, (1970), 1–13.

Bellanger, M., Ars, J.-M., Auxietre, J.-L., Hautot, S., Hermant, B Tarits, P.: High temperature geothermal resources of crustal fault zones : a dedicated approach, 79th *EAGE* Conference and Exhibition-Workshops (2017).

Gola, G., Bertini, G., Bonini, M., Botteghi, S., Brogi, A., De Franco, R., Dini, A., Donato, A., Gianelli, G., Liotta, D., et al.: Data integration and conceptual modelling of the Larderello geothermal area, Italy. *Energy Procedia,* **125**, (2017), 300–309.

Granet, M., Wilson, M., & Achauer, U.: Imaging a mantle plume beneath the French Massif Central, *Earth and Planetary Science Letters*, ***136*** (3-4), (1995), 281-296.

Hautot, S., Single, R., Watson, J., Harrop, N., Jerram, D., Tarits, P., Whaler, K., Dawes, D.: 3-D magnetotelluric inversion and model validation with gravity data for the investigation of flood basalts and associated volcanic rifted margins, *Geophysical Journal International,* **170** (3), (2007), 1418–1430.

Hautot, S., Tarits, P., Whaler, K., Le Gall, B., Tiercelin, J.-J., Le Turdu, C.: Deep structure of the Baringo rift basin (central Kenya) from three-dimensional magnetotelluric imaging : Implications for rift evolution, *Journal of Geophysical Research : Solid Earth*, **105** (B10), (2000), 23493–23518.

Levshin, AL, Y. T., , Its, E., Lander, A., Bukchin, B., Barmin, M., Ratnikova, L.: Seismic surface waves in a laterally inhomogeneous earth, *Springer Science & Business Media*, **9,** (1989).

Moeck, I. S.: Catalog of geothermal play types based on geologic controls. *Renewable and Sustainable Energy Reviews*, **37**, (2014), 867–882.

Mordret, A., Landes, M., Shapiro, N., Singh, S., & Roux, P.: Ambient noise surface wave tomography to determine the shallow shear velocity structure at Valhall: depth inversion with a neighbourhood algorithm, *Geophys. J. Inter.*, **198**, (2014), 1514–1525.

NASA: Aster global digital elevation model 45.7n, 2.7e. nasa jpl, (2009). URL https://doi.org/10.5067/aster/astgtm.002

Piña-Varas, P., Dentith, M.: Magnetotelluric data from the Southeastern Capricorn Orogen, Western Australia: an example of widespread out-of-quadrant phase responses associated with strong 3-D resistivity contrasts, *Geophysical Journal International*, **212** (2), (2018), 1022–1032, https://doi.org/10.1093/gji/ggx459

Press, W., Teukolsky, S., Vetterling, W., Flannery, B.: Numerical Recipies 3rd edition. Cambridge University Press (2007).

Roche, V., Sternai, P., Guillou-Frottier, L., Jolivet, L., Gerya, T.: Eastern Mediterranean geothermal resources and subduction dynamics, In : *EGU General Assembly Conference Abstracts*, **19**, (2017), 13427.

Shapiro, N. M., Campillo, M.: Emergence of broadband rayleigh waves from correlations of the ambient seismic noise. *Geophysical Research Letters,* **31** (7), (2004).

Wathelet, M.: Array recordings of ambient vibrations : surface wave inversion, Theses, Université de Liège (2005).